Anion Rotation and Cation Diffusion in Low-Temperature Sodium Orthophosphate: Results from Solid-State NMR

Michael Witschas and Hellmut Eckert*

Institut für Physikalische Chemie, Westfälische Wilhelms-Universität Münster, Schlossplatz 4-7, D-48149 Münster, Germany

Hans Freiheit and Andrew Putnis

Institut für Mineralogie, Westfälische Wilhelms-Universität Münster, Corrensstrasse, D-48149 Münster, Germany

Gaby Korus and Martin Jansen

Max-Planck Institut für Festkörperforschung, Heisenbergstrasse 1, D-70569 Stuttgart, Germany

Received: October 4, 2000; In Final Form: February 6, 2001

Numerous ionic crystals are known in which both cations and anions possess considerable mobility in the solid state. During the past decade, there has been considerable controversy about the question of whether cationic and anionic motion can be dynamically coupled in such materials. This issue has been studied recently on the plastic crystalline material high-temperature (HT-) Na_3PO_4, which forms from the low-temperature modification in a first-order phase transition at a temperature near 600 K. In the present study, the dynamics of the low-temperature phase have been characterized comprehensively by complementary NMR methods. Temperature-dependent ^{17}O NMR line shape analyses indicate that the phosphate ions undergo 3-fold rotation on the time scale of milliseconds. There appears to be one preferred axis of rotation, however. Variable-temperature ^{23}Na and ^{31}P NMR spectra reveal further that the sodium cations exhibit considerable mobility. Both anionic and cationic motion appear to be jointly thermally activated and are characterized by correlation times of comparable magnitude. At temperatures about 70 K below the phase transition, diffuse diffraction peaks observed in X-ray powder diffraction data indicate the appearance of local clusters possessing the symmetry of the high-temperature phase. The strongly increased thermal volume expansion coefficient and the observation of excess specific heat within this temperature range suggest that both the cations and the anions exhibit strongly accelerated dynamics within these domains. The number of nuclei contributing to these domains are quantified on the basis of ^{17}O and ^{23}Na NMR line shape and nutation analyses. The combined experimental evidence suggests strong dynamic coupling between anion and cation motion in low-temperature (LT-) Na_3PO_4.

Introduction

Current fundamental research in the solid electrolyte area focuses at developing a microscopic understanding of ion transport in disordered solids. In such materials the structural framework surrounding the mobile ions may be rigid (as in crystalline or glassy solid electrolytes) or flexible and highly mobile (as in polymer electrolytes). A special intermediate situation of particular interest holds for a number of lithium and sodium salts with polyatomic anions such as SO_4^{2-} or PO_4^{3-}. These compounds undergo phase transitions at elevated temperatures resulting in plastic crystals combining high translational cationic mobility with dynamic anion disordering. For two decades, researchers have discussed the possibility that the transport of the cations is dynamically coupled to the reorientational motion of the anions.[1] This concept, labeled as a paddle-wheel mechanism, has met with strong support,[2−6] opposition,[7−10] and incisive rediscussion.[11] Most recently, a strong case in favor of the paddle-wheel mechanism has been presented for the high-temperature phase of sodium orthophosphate, HT-Na_3PO_4. From a combination of NMR, inelastic neutron scattering, and electrical conductivity measurements it could be shown that anion rotation and cation transport appear to be highly correlated in this material over a wide range of time and temperature scales.[12,13]

The present study is devoted to the low-temperature phase of Na_3PO_4 which is thermodynamically stable at temperatures below 600 K. The crystal structure of this compound was solved from X-ray and neutron powder diffraction data in the space group $P\bar{4}21c$.[14] The unit cell contains eight equivalent phosphate tetrahedra whose orientations are perfectly ordered, as illustrated in Figure 1. There are five distinct sites for the sodium cations, which have different occupancy factors, and whose individual line shapes can be resolved by ^{23}Na high-resolution solid-state NMR.[15]

The goal of the present study is to characterize anion and cation dynamics in this phase and to see whether the feature of correlated motion also holds in the low-temperature phase. The motion of the phosphate ions is studied by temperature- and frequency-dependent ^{17}O NMR line shape data on isotopically labeled material. To clarify the predictive significance of these

* Author to whom correspondence should be addressed.

10.1021/jp003635t CCC: $20.00
Published on Web 06/20/2001

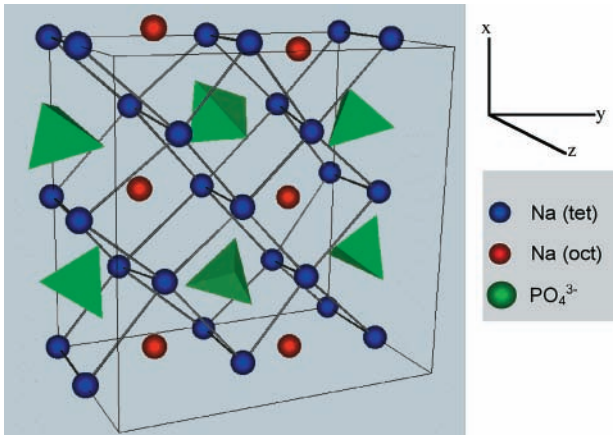

Figure 1. Crystal structure of LT-Na_3PO_4. For simplicity, only half of the unit cell is shown along the *z* direction.

NMR data, we contrast the experimental spectra with simulated data for distinct dynamical scenarios. Complementary information concerning the cation motion in this time window is available from ^{23}Na and ^{31}P solid-state NMR line shape characteristics. Furthermore, insights about the nature of the LT−HT transition will be sought from the combined interpretation of the NMR data with results from X-ray powder diffraction and differential scanning calorimetry. Based on the combined experimental evidence, the data will present clear manifestations of the previously discussed dynamic coupling between anion and cation motion in the low-temperature phase of this material.

Fundamental Concepts and Methodology

NMR line shapes in rigid solids are dominated by the anisotropy of static interactions, which the nuclei experience with local magnetic and electrical fields owing to a number of distinct interaction mechanisms. For each nuclear species a general description of the total spin Hamiltonian is

$$\mathbf{H} = \mathbf{H}_Z + \mathbf{H}_{cs} + \mathbf{H}_{dhomo} + \mathbf{H}_{dhetero} + \mathbf{H}_Q \qquad (1)$$

consisting of the dominant Zeeman term ($\mathbf{H}_Z$) and smaller terms describing the effects of chemical shift, homo- and heteronuclear dipole−dipole interactions, and (for $I > {}^1/_2$ nuclei) nuclear electric quadrupolar couplings. For each type of interaction, the orientational dependence of the NMR resonance frequency can be calculated by applying standard perturbation theory. The static NMR line shape then results when the corresponding powder average is formed.

The line shape is modified by stochastic processes such as diffusion or molecular jump rotation occurring on the inherent time scale of the interaction in question. Such processes are characterized by a spectral density function, which corresponds to the Fourier transform of the autocorrelation function, which in many cases decays exponentially, $G(\tau) = e^{-\tau/\tau_c}$. Here τ_c is the motional correlation time, whose inverse describes the rate with which the anisotropic internal NMR Hamiltonian fluctuates, resulting in the decay of the correlation function. When τ_c^{-1} becomes comparable to the spectral dispersion caused by the anisotropic spin interactions, these fluctuations cause motional narrowing under the condition $\Delta\omega \approx \tau_c^{-1}$. Since, in general, $\Delta\omega$ is on the order of several kilohertz, the static NMR line shape will be sensitive to motional processes with correlation times in the millisecond region. Within this time window, characteristic line shapes can be observed, from which the motional type and the corresponding correlation times can be extracted.

In LT- Na_3PO_4, the anisotropic rigid lattice line shape of the spin-$^1/_2$ nuclide ^{31}P is dominated by homo- and heteronuclear dipole−dipole couplings with the surrounding ^{31}P and ^{23}Na spins, whereas the chemical shift anisotropy makes only a negligible contribution. The multispin dipolar coupling is most efficiently described in terms of a second moment M_{2D}, according to[16]

$$M_{2D} = \left(\frac{\mu_0}{4\pi}\right)^2 \hbar^2 \left\{ \frac{3}{5}\gamma_P{}^4 I(I+1) \sum_{P_j} r_{P-P_j}{}^{-6} + \frac{4}{15}\gamma_P{}^2 \gamma_{Na}{}^2 S(S+1) \sum_{Na_j} r_{P-Na_j}{}^{-6} \right\} \qquad (2)$$

Here, I and S are the spin quantum numbers of ^{31}P ($^1/_2$) and ^{23}Na ($^3/_2$), γ_P and γ_{Na} are the corresponding gyromagnetic ratios, and r are internuclear distances. All the other symbols have their usual meanings. Typically, Gaussian-shaped resonance curves are observed, whose full width at half-height (fwhh) relates to the second moment according to

$$\Delta\nu = \frac{\sqrt{M_{2D}\, 8 \ln 2}}{2\pi} \qquad (3)$$

As discussed below, the temperature-dependent evolution of $M_{2D}(^{31}P)$ can provide insight into the details of both cation and anion motion in this material.

The ^{17}O NMR line shapes in HT-Na_3PO_4 are dominated by $\mathbf{H}_Q$, while contributions from the other types of interactions can be neglected. Due to large quadrupolar splittings, only the central $|^1/_2\rangle \leftrightarrow |^{-1}/_2\rangle$ transition is observable. Second-order quadrupolar effects render the resonance frequency of this transition orientationally dependent. For axially symmetric electric field gradients, one finds[17]

$$\omega_{1/2,-1/2} - \omega_0 = \frac{3\pi C_Q{}^2}{4I^2(2I-1)^2\nu_0}\left\{I(I+1) - \frac{3}{4}\right\} \times \left\{-\frac{27}{8}\cos^4\varphi + \frac{15}{4}\cos^2\varphi + \frac{3}{8}\right\} \qquad (4)$$

In this expression, ν_0 and C_Q are the resonance frequency and the nuclear electric quadrupolar coupling constant, while the angle φ specifies the orientation of the electric field gradient (EFG) principal axis relative to the magnetic field direction. Ab initio calculations carried out for the sulfate ion suggest that the ^{17}O EFG is dominated by the S−O bonds, whereas the effect of the positive charges of the sodium ions close to oxygen is negligible.[18] By analogy, we make the same assumption here for the phosphate ion. Thus, we can identify the EFG principal axis direction with the oxygen−phosphorus bond. This assumption is supported by the ^{17}O NMR spectrum measured at room temperature, revealing that the EFG is axially symmetric (see below). Detailed inspection indicates, however, that the effect of the ^{17}O−^{31}P dipole−dipole interaction cannot be neglected. Since both the dipolar and quadrupolar tensors are coincident in the present case, this frequency correction is simply given by

$$\Delta\omega_{IS} = {}^1/_2 D(1 - 3\cos^2\varphi) \qquad (5)$$

with

$$D = (\mu_0/4\pi)\hbar\gamma_P\gamma_O r_{P-O}{}^{-3} \qquad (6)$$

Anisotropic reorientational jumps of the phosphate ions make the orientation of the P−O bond (and hence the ^{17}O resonance frequency) time-dependent, resulting in distinct line shape changes on the appropriate time scale. These effects can be computed from chemical exchange theory, by use of the master equation:[19]

$$d\mathbf{G}/dt = \mathbf{G}(i\boldsymbol{\omega} + \boldsymbol{\Pi}) \quad (7)$$

Here the matrix $\boldsymbol{\Pi}$ specifies the exchange rates connecting sites α, β, etc., having resonance frequencies ω_α, ω_β, etc. The dimensionality of $\boldsymbol{\Pi}$ reflects the number of independent positions involved in the exchange. The solution of eq 7

$$G(t) = \mathbf{W}\cdot\exp[(i\boldsymbol{\omega} + \boldsymbol{\Pi})t] \quad (8)$$

includes $\mathbf{W} = G(0)$ as the static occupancies. The time domain signal of eq 8 is subsequently Fourier-transformed to yield the frequency domain spectrum:

$$I(\omega) = Re\int_0^\infty \mathbf{W}\cdot\exp[\{i(\boldsymbol{\omega} - \omega\mathbf{E}\} + \boldsymbol{\Pi}\}t]\cdot\mathbf{1}\, dt = Re(\mathbf{W}\cdot\mathbf{A}^{-1}\cdot\mathbf{1}) \quad (9)$$

Here, $\mathbf{E}$ is the unity matrix and $\mathbf{1}$ is a vector with components 1. Since in the present case, the spectra were obtained by the Hahn spin−echo method, the time domain signal and its Fourier transform are calculated according to[20,21]

$$K(t,\tau) = \mathbf{W}\cdot\exp[i(\boldsymbol{\omega} + \boldsymbol{\Pi})\tau]\exp[(i\boldsymbol{\omega} + \boldsymbol{\Pi})(t - \tau)] \quad (10)$$

and

$$I_E(\omega) = Re\int_0^\infty K(t,\tau)\cdot\exp[-i\omega\mathbf{E}(t - 2\tau)]\cdot\mathbf{1}\, dt \quad (11)$$

respectively. This calculation accounts for the intensity losses and line shape distortions expected if the correlation times of the motional process under consideration are comparable to the spin−echo delay time τ used in the experiment.

Finally, the resulting solid-state NMR powder line shape is then obtained numerically,[22] by executing the integral of eq 11 for many orientations of the phosphate ion rotation axis θ and by subsequently weighting the contribution of each orientation with the θ−probability distribution. The result is a simulated line shape based on an assumed reorientational model, which can then be calculated systematically as a function of exchange rate $\pi_{\alpha\beta}$. Drastic line shape effects are particularly observed within the regime $\Delta\omega/\pi_{\alpha\beta} \approx 1$; at larger rates, a constant line shape is reached eventually (fast exchange limit). Fast isotropic motion produces Lorentzian line shapes.

Numerical analysis of the temperature-dependent ^{23}Na NMR spectra is made impossible by the severe overlap of five different spectral contributions. However, additional information on the anion and cation dynamics is available here from nutation NMR spectroscopy. As discussed in detail elsewhere,[23] if the first-order quadrupolar splittings are so large that only the central $|^1/_2\rangle \leftrightarrow |^{-1}/_2\rangle$ coherence is excited, the effective nuclear Larmor frequency in the rotating frame is modified according to

$$\omega_1 = (I + {}^1/_2)\omega_{rf} \quad (12)$$

Here ω_{rf} corresponds to the nutation frequency measured under nonselective excitation of all of the Zeeman transitions, as measured for a liquid sample or for a solid sample in which quadrupolar couplings vanish either owing to perfect cubic symmetry or because of dynamical averaging by motional processes. Thus, the method is well-suited for probing atomic and/or molecular dynamics. While immobile nuclei with large stationary quadrupolar coupling constants exhibit nutation frequencies given by eq 12, sufficiently mobile nuclei exhibit nonselective excitation characteristics. For such ^{23}Na nuclei ($I = {}^3/_2$) eq 12 predicts effective 90° lengths twice as long as for the nuclei experiencing strong static electric field gradients in rigid solids.

Experimental Section

Sample Preparation and Characterization. Powder samples of pure Na_3PO_4 were obtained by solid-state reaction of Na_2CO_3 and $Na_4P_2O_7$ at 800 °C for 48 h.[14] Sample purity was confirmed by X-ray diffraction. Samples were kept dry during all stages of handling and measurement. For the purpose of the NMR studies, ^{17}O-enriched material was prepared according to the reaction sequence [24] $2Na + H_2O^* \rightarrow Na_2O^* + H_2$ and $Na_2O + Na_4P_2O_7 \rightarrow 2Na_3PO_4$, resulting in a 4.1% enrichment level in the final product. In the first step, isotopically enriched Na_2O was prepared within a Ni crucible enclosed in a quartz tube under Ar atmosphere, by slowly warming a mixture of excess distilled sodium and CO_2-free $H_2{}^{17}O$ (33% enrichment) to room temperature. Hydrogen gas formed during this reaction was allowed to escape through a Hg valve. After 4 days at room temperature the reaction was brought to completion by heating the ampule to 350 °C. Residual Na was distilled off at 400 °C in high vacuum. The ^{17}O-enriched Na_2O material (98.5% purity) was mixed with $Na_4P_2O_7$ in a stoichiometric ratio under Ar atmosphere. The mixture was subsequently transferred to an Ag crucible, which was enclosed in a glass ampule and heated at 400 °C for 1 week. The lattice constants were measured over a temperature range between 293 and 800 K, using an Enraf-Nonius Guinier-Simon camera and Cu $K\alpha_1$ radiation (Philips PW 1130 generator, 40 kV/30 mA). Silicon was used as internal standard. The temperature dependence of the specific heat was measured by differential scanning calorimetry with a Netzsch DSC-200 system.

Solid-State NMR Studies. Solid-state NMR studies were carried out on Bruker CXP-200 and CXP-300 spectrometers upgraded with a TECMAG pulse programmer and data acquisition system. Solid-state NMR line shapes were recorded at the Larmor frequencies of 81.0 MHz for ^{31}P (4.65 T magnet), 79.4 MHz for ^{23}Na (7 T magnet), and 40.6 MHz for ^{17}O (7 T magnet). For ^{31}P and ^{23}Na, the 90° pulse lengths were 8 μs; for ^{17}O, the nonselective 90° pulse length was 18 μs. For temperatures below ambient, a commercial Bruker probe was used, whereas all of the high-temperature experiments utilized home-built solenoidal variable-temperature probes with a water-cooled jacket. Temperature gradients within the probes were carefully mapped out, and the effects of thermal gradients across the samples were minimized by spectroscopic measurements as a function of sample length. Two-dimensional ^{23}Na nutation NMR studies were obtained within the temperature range 526−586 K, under the following conditions: nonselective nutation frequency 20 kHz, pulse length increment 2 μs, and 128 spectra in the t_1 domain. For ^{17}O NMR, the detection sensitivity was insufficient to measure the full 2D nutation spectra. In this case, a Hahn spin−echo (90°−τ−180°) pulse sequence was applied, with selective 90° pulses according to eq 12. In addition, the intensity of a nonselective Hahn echo was measured for comparison.

^{17}O NMR Line Shape Simulations for Different Reorientational Models. NMR powder line shapes were calculated with the following algorithm in Mathematica 3.0: (1) choice of a specific orientation of the P−O bond and computation of the

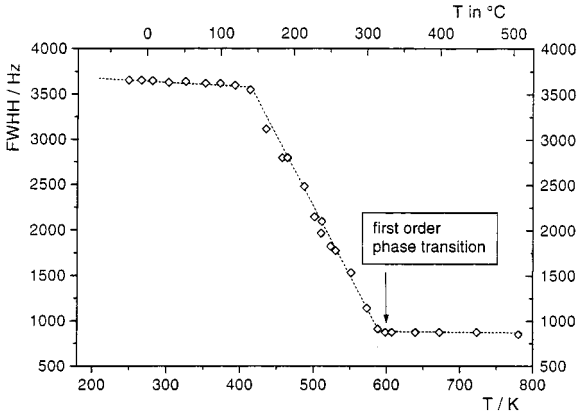

Figure 2. Temperature dependence of the ^{31}P NMR line width (full width at half-height) of LT-Na_3PO_4. The arrow denotes the phase transition temperature.

^{17}O resonance frequencies for all of the four oxygen atoms, by use of eqs 4−6; (2) calculation of the decaying part of the ^{17}O Hahn spin−echo from eq 10 and weighting according to its probability of occurrence in a powder sample; (3) incrementation of the orientation angles and recalculation, for a total of 2400 increments; and (4) exponential multiplication and Fourier transformation. A simulation map of reorientation rates ranging from 100 Hz to 3 MHz was created. Visual comparison of the experimental spectrum with this simulation map resulted in the estimation of a reorientation rate for each temperature studied. Least-squares fitting routines were not used because of problems arising from baseline artifacts and low signal-to-noise ratios.

Results, Data Analysis, and Interpretation

^{31}P NMR Line Shape. Temperature-dependent measurements of the static ^{31}P NMR spectra show purely Gaussian shapes at temperatures below 420 K and above 573 K; in the temperature interval in between, a mixture of equal Gaussian and Lorentzian fractions gave the best fit to the experimental spectra. The corresponding fwhh values are shown in Figure 2. The Gaussian rigid lattice line width of low-temperature Na_3PO_4 is measured to be 3600 Hz, in good agreement with the van Vleck value of 3300 Hz from eq 2. The small discrepancy is attributed to a contribution arising from the chemical shift anisotropy, since it is known that in low-temperature sodium orthophosphate the PO_4^{3-} anions show slight deviations from ideal tetrahedral symmetry.

As the temperature is increased within the interval 373 K < T < 573 K, motional narrowing effects become clearly observable in the static ^{31}P NMR spectra. The line width is reduced, and its shape becomes partially Lorentzian. Finally, at a temperature just below the phase transition temperature, a constant Gaussian line width of 850 Hz is measured. This value is in excellent agreement with that calculated from part a of eq 2 quantifying the homonuclear dipolar interactions between the immobile ^{31}P nuclei: when the known internuclear $^{31}P-^{31}P$ distances in the crystal structure are taken into account, the theoretical line width is 815 Hz. Thus, the ^{31}P spectra clearly document the thermal activation of Na^+ motion on the NMR time scale, producing successive averaging of the heteronuclear $^{23}Na-^{31}P$ dipole−dipole interactions. Near the phase transition temperature, the sodium ions can be viewed as nearly isotropically mobile.

^{17}O NMR Line Shape and Nutation Characteristics. Figure 3 shows the static ^{17}O NMR spectrum at room temperature. The line shape was simulated according to eq. (4−6), assuming

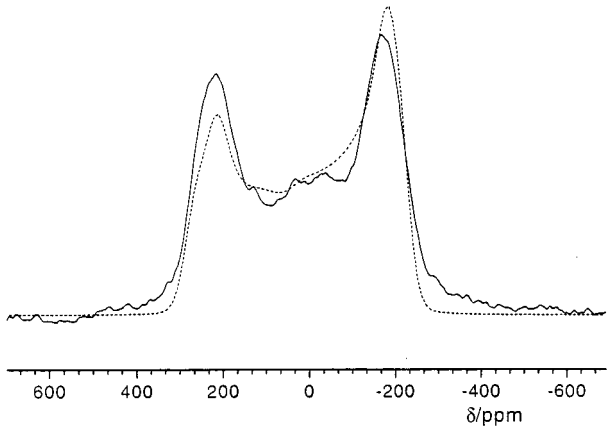

Figure 3. Static ^{17}O solid-state NMR spectrum of LT-Na_3PO_4. The dotted line is a simulation based on a quadrupolar coupling constant of 4.6 MHz and a $^{17}O-^{31}P$ dipolar coupling constant of 11.2 kHz. Coincident quadrupolar and dipolar tensors are assumed.

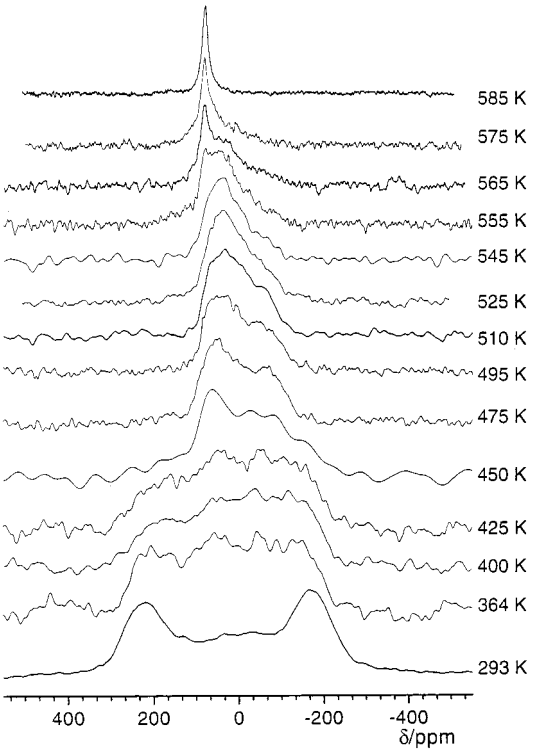

Figure 4. Temperature dependence of the ^{17}O NMR spectra of LT-Na_3PO_4. The spectrum at 585 K was obtained with nonselective single-pulse excitation.

a jump rate value of 0. A P−O internuclear distance of 1.54 Å was used, resulting in a dipole−dipole coupling constant of 11.2 kHz. Optimum agreement with the experimental spectrum was observed by assuming $C_Q(^{17}O) = 4.6$ MHz and $\eta = 0$. Figure 4 shows the spectra as a function of temperature. At temperatures above 364 K, characteristic motional narrowing effects become clearly visible, signifying the onset of phosphate motion. In this figure, all of the spectra were obtained with the selective Hahn echo pulse sequence; however, at temperatures above 510 K, a noticeable intensity loss was clearly observed in these experiments. At the same time, complementary experiments using the nonselective Hahn spin−echo sequence reveal the appearance of an isotropic species (Lorentzian line shape), which gains in intensity as the temperature is increased further. Since the line shapes of the selectively and the nonselectively excited ^{17}O signals are different, their distinct contributions to the

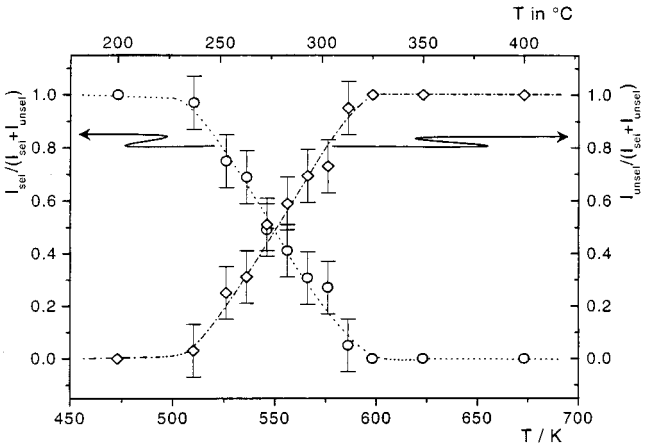

Figure 5. Temperature dependence of the fractional contributions of the ^{17}O NMR line shape components in LT-Na_3PO_4 that are selectively excited (left axis) and nonselectively excited (right axis).

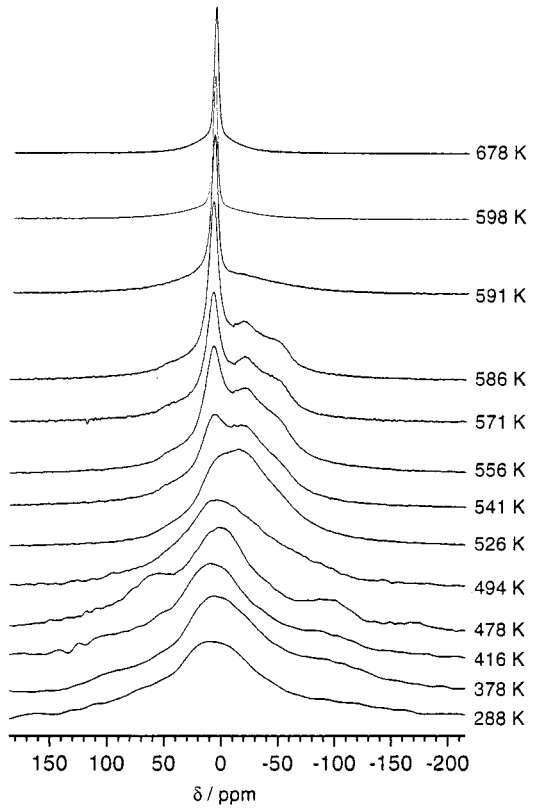

Figure 6. Temperature dependence of the ^{23}Na NMR line shape in LT-Na_3PO_4.

spectrum are separable. Figure 5 summarizes the temperature dependence of the fractional intensities of both signal components. In generating this figure, the data have been internally normalized at each temperature to account for the fact that the appearance of the nonselective component produces an increase in the absolute intensity. At temperatures near the phase transition, the signal component having selective excitation characteristics is no longer observed, and only a (nonselectively excited) Lorentzian ^{17}O NMR line shape is observed.

^{23}Na NMR Line Shape and Nutation Characteristics. Figure 6 shows the variable-temperature ^{23}Na NMR spectra. At low temperatures the spectra are dominated by second-order quadrupolar broadening; however, a rather ill-defined line shape is observed, arising from the superposition of the respective NMR powder patterns from five crystallographically independent sodium sites. As the temperature is raised above 526 K,

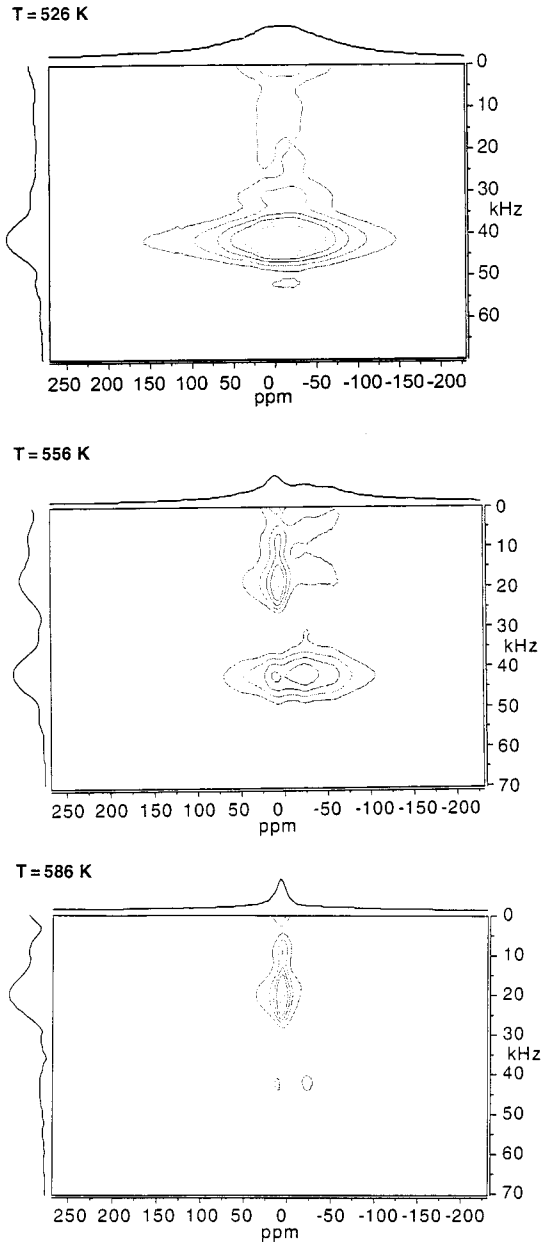

Figure 7. Selected ^{23}Na 2D nutation NMR spectra of LT-Na_3PO_4. At 526 K the majority of sodium species are detected by selective excitation (eq 12), whereas at 586 K most of the sodium nuclei are nonselectively excited.

an isotropic line shape component becomes evident. The nutation spectra (Figure 7) illustrate that the low-temperature spectra represent the line shapes of the selectively excited $|^1/_2\rangle \leftrightarrow |^{-1}/_2\rangle$ transition, whereas the isotropic component observed at the higher temperatures is characterized by nonselective excitation characteristics. For this component, the quadrupolar splittings have collapsed owing to fast sodium motion. As in the case of the ^{17}O spectra (Figure 5), both line shape contributions are separable. As Figure 8 illustrates, the fractional intensity of the nonselectively excited line shape component increases with increasing temperature, and near the phase transition temperature it is the sole sodium species present. The close analogy observed for the ^{17}O and ^{23}Na line shape and nutation characteristics as a function of temperature is most significant as discussed below.

Bulk Characterization. Thermal expansion often provides useful information on phase transitions as in many cases it can

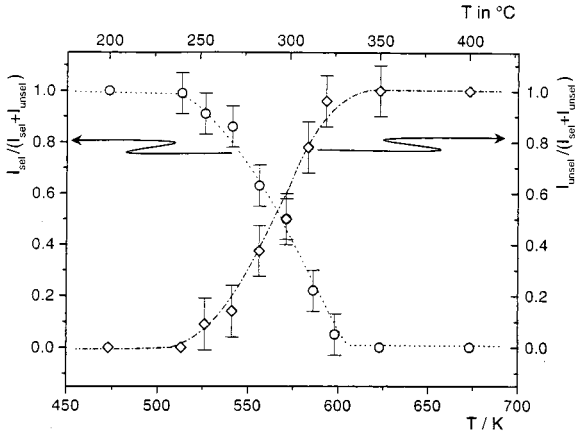

Figure 8. Temperature dependence of the fractional contributions of the ^{23}Na NMR line shape components in LT-Na_3PO_4 that are selectively excited (left axis) and nonselectively excited (right axis).

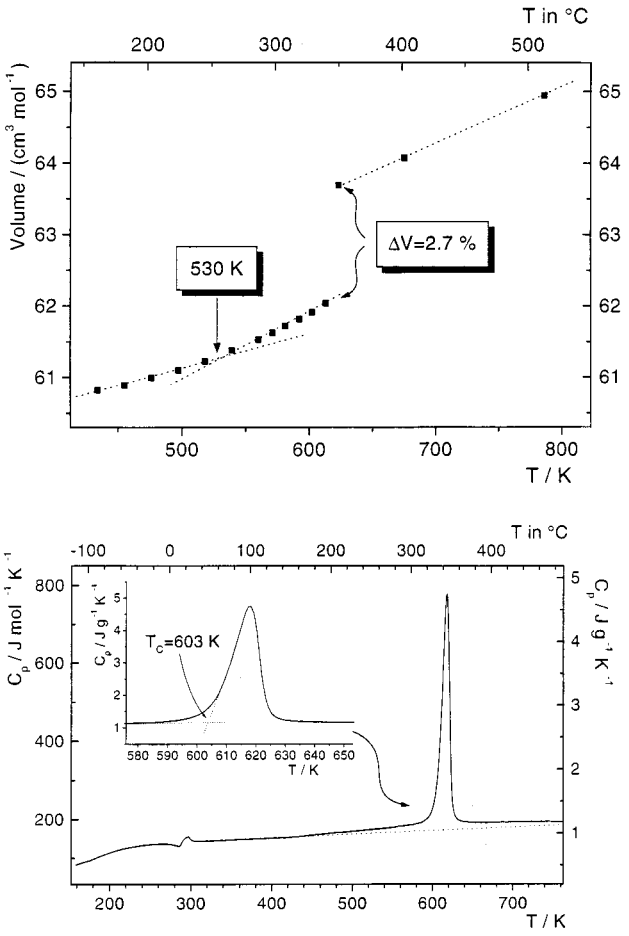

Figure 9. (a, top panel) Temperature dependence of the molar volume of LT-Na_3PO_4. (b, bottom panel) Temperature dependence of the molar heat capacity of LT-Na_3PO_4. The dotted line is the baseline. Note the premonitory effect noticeable as an excursion from the baseline above 500 K.

be directly related to structural changes. The upper panel of Figure 9 shows the temperature evolution of the molar volume, as calculated from the lattice parameters determined by X-ray powder diffraction:

$$V_{mol} = N_A \frac{a^2 c}{Z} \qquad (13)$$

where a and c are the tetragonal lattice parameters, N_A is the Avogadro constant, and Z is the number of formula units in the unit cell. Lattice parameters were obtained by standard least-squares fits to 20 Bragg reflections. At the phase transition, the molar volume expands by 2.7%, and the high-temperature phase has a relative volume expansion coefficient of 12.0×10^{-5} K^{-1}.

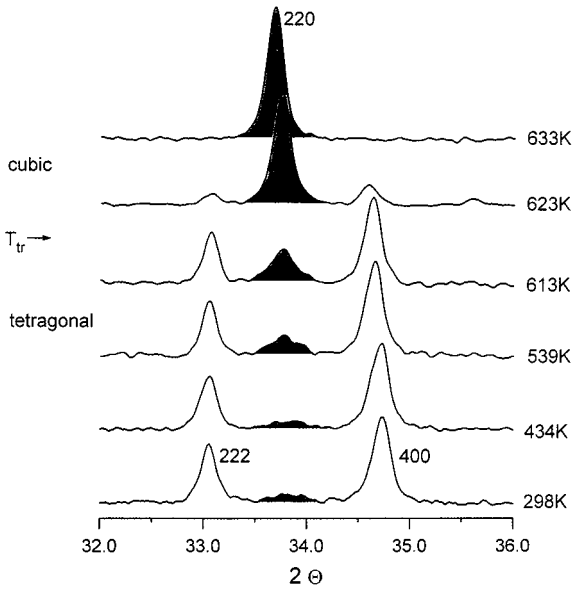

Figure 10. Temperature dependence of X-ray powder diffraction data ($32° < 2\Theta < 36°$).

In LT-Na_3PO_4 the data reveal linear expansion of 10.5×10^{-5} K^{-1} at temperatures below 525 K; at higher temperatures, the curve bends visibly upward, indicating an anomalous increase in molar volume with a thermal expansion coefficient of 14.5×10^{-5} K^{-1}, which is significantly larger than in HT-Na_3PO_4. However, no indications for a symmetry change below the tetragonal-to-cubic phase transition are found in the powder patterns. As the lower panel of Figure 9 illustrates, this increase is paralleled by a noticeable specific heat increase in the same temperature region, suggesting the onset of atomic/molecular motion in a way that the average tetragonal symmetry is retained.

A further characteristic feature of the diffraction pattern is the occurrence of a broad diffuse peak located between the tetragonal 400 and the 222 Bragg reflections at $2\theta \approx 33.7°$, which begins to sharpen at about 525 K and becomes identical with the cubic 220 reflection at the phase transition (Figure 10). However, no disappearance of the diffuse intensity is observed after several heating and cooling cycles, indicating the survival of cubic microdomains in the low-temperature phase, down to nearly 100 K below the phase transition temperature. The intensity with which these diffuse peaks were observed was sample-dependent, and in ultrapure samples, the peaks were found to be absent at 298 K. Thus, it appears that the hysteresis behavior is favored by the presence of small amounts of impurities.

Discussion

Reorientational Models for the Phosphate Anions. The characteristic ^{17}O NMR line shapes observed within the temperature range 425 K $< T <$ 545 K contain important information about the mechanism of anion reorientation. By use of eq 11, different motional scenarios of the phosphate groups can be tested against experimental data.

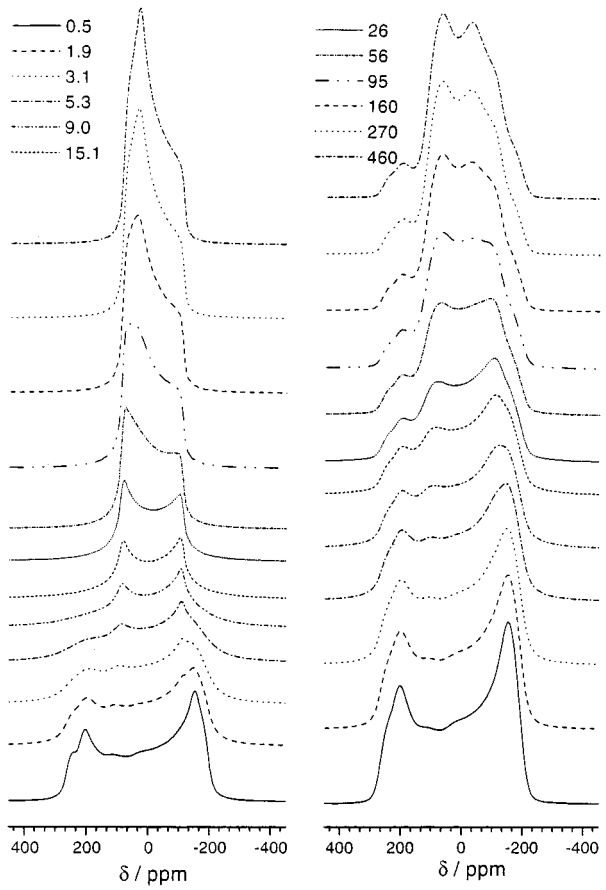

Figure 11. Simulated ^{17}O NMR line shapes for two reorientational models for the phosphate ions for 12 different reorientation rates (see legend): (right panel) 3-fold rotation about a single fixed axis; (left panel) 3-fold rotation about all four C_3 axes.

Since the line shape reveals a residual anisotropy even at high temperatures close to the phase transition, the possibility of an isotropic rotational diffusion of the phosphate ions is ruled out by the experimental data for all temperatures $T < 525$ K. Such a mechanism would result in a Lorentzian signal with no residual anisotropy observable, as is indeed observed for the ^{17}O NMR spectrum of the high-temperature phase.[13b] Alternatively, we can consider the case of a jump rotation about a fixed 3-fold axis, corresponding to one of the P−O− bonds of the tetrahedron. In this case, the exchange matrix used to solve eq 11 possesses the form

$$\begin{bmatrix} -2\Pi & \Pi & \Pi & 0 \\ \Pi & -2\Pi & \Pi & 0 \\ \Pi & \Pi & -2\Pi & 0 \\ 0 & 0 & 0 & 0 \end{bmatrix}$$

This mechanism would produce a temperature-dependent line shape evolution as shown in the right-hand panel of Figure 11a. One of the four oxygen atoms would remain stationary and therefore experience no modulation of its electric field gradient whereas the signals of the other three oxygen atoms would appear partially narrowed. In contrast to this scenario, the much more drastic line narrowing observed in the experimental data suggests that all of the four oxygen atoms are involved in the anionic reorientation. A much more realistic representation of the experimental spectra can be obtained by assuming rotations about all four C_3 axes with equal rates (see left-hand panel of Figure 11). In this case, the exchange matrix is written as

$$\begin{bmatrix} -4\Pi & {}^4/_3\Pi & {}^4/_3\Pi & {}^4/_3\Pi \\ {}^4/_3\Pi & -4\Pi & {}^4/_3\Pi & {}^4/_3\Pi \\ {}^4/_3\Pi & {}^4/_3\Pi & -4\Pi & {}^4/_3\Pi \\ {}^4/_3\Pi & {}^4/_3\Pi & {}^4/_3\Pi & -4\Pi \end{bmatrix}$$

Detailed comparison with the experimental data reveals the need for additional refinement. In fact, the best agreement with the experimental data is obtained by assuming the existence of a preferred axis of reorientation (with rate Π), whereas the rotation about the other three C_3 axes of the tetrahedron occurs at a distinctly lower rate Ω. In this case, the exchange matrix takes the form

$$\begin{bmatrix} -2\Pi - 2\Omega & \Pi + {}^1/_3\Omega & \Pi + {}^1/_3\Omega & {}^4/_3\Pi \\ \Pi + {}^1/_3\Omega & -2\Pi - 2\Omega & \Pi + {}^1/_3\Omega & {}^4/_3\Pi \\ \Pi + {}^1/_3\Omega & \Pi + {}^1/_3\Omega & -2\Pi - 2\Omega & {}^4/_3\Pi \\ {}^4/_3\Pi & {}^4/_3\Pi & {}^4/_3\Pi & -4\Omega \end{bmatrix}$$

Figure 12 juxtaposes the experimental data (left panel in each set of three) with visual best-fit simulations of this model (middle panel in each set of three). An alternate scenario, resulting also in the relocation of all four of the oxygen atoms, is based on 180° jumps about one of the C2 axes of the tetrahedron (2 × 2 matrix, rate Φ). The simulations for this model are included in Figure 12 (right panel in each set of three). Clearly this model cannot suitably account for the experimental spectra observed. Altogether, the results of the present study indicate that temperature-dependent ^{17}O NMR spectra are very sensitive to the details of the phosphate reorientation in LT-Na_3PO_4. The data suggest anionic reorientation about a preferred C_3 axis with a rate Π, and reorientations about the other C_3 axes at distinctly smaller rates Ω. From a plot (Figure 13) of Π against inverse temperature, we obtain an activation energy of 0.65 + 0.03 eV.

Dynamic Coupling of Anion and Cation Motion. With respect to the issue of correlated cation and anion motion, two experimental findings are significant: First of all, the joint inspection of the ^{17}O and the ^{31}P NMR temperature dependences reveals two distinct dynamic regimes: Within the temperature interval 300 K < T < 425 K, only slight narrowing effects are observable in the spectra of both nuclear species, revealing that both cation and anion motion are slow on the NMR time scale. At temperatures above 425 K, dramatic narrowing of the ^{17}O spectra is observed *simultaneously* with the onset of a significant modulation of the ^{31}P−^{23}Na dipole−dipole interaction strength. This confluence of effects is illustrated in Figure 14, where the temperature dependences of the ^{31}P and ^{17}O NMR line widths are plotted jointly. By use of the Waugh−Fedin expression

$$E_A\ (\text{kJ/mol}) = 0.156 T_c \qquad (14)$$

with T_c as the critical (onset) temperature, an activation energy of 0.69 eV can be estimated, which is in good agreement the value obtained from the ^{17}O NMR line shape simulation.

The second point concerns the joint appearance of nonselectively excited ^{17}O and ^{23}Na NMR signals arising from nuclei with high atomic/molecular mobilities. In both cases, these species start appearing at temperatures above 525 K and their contribution increases to 100% at temperatures near the phase transition. At 525 K, the phosphate ions are already characterized by significant mobility: the rates of the molecular rotations about the four C_3 axes indicate the process is fast on the NMR time scale. If this were the only anionic motion occurring,

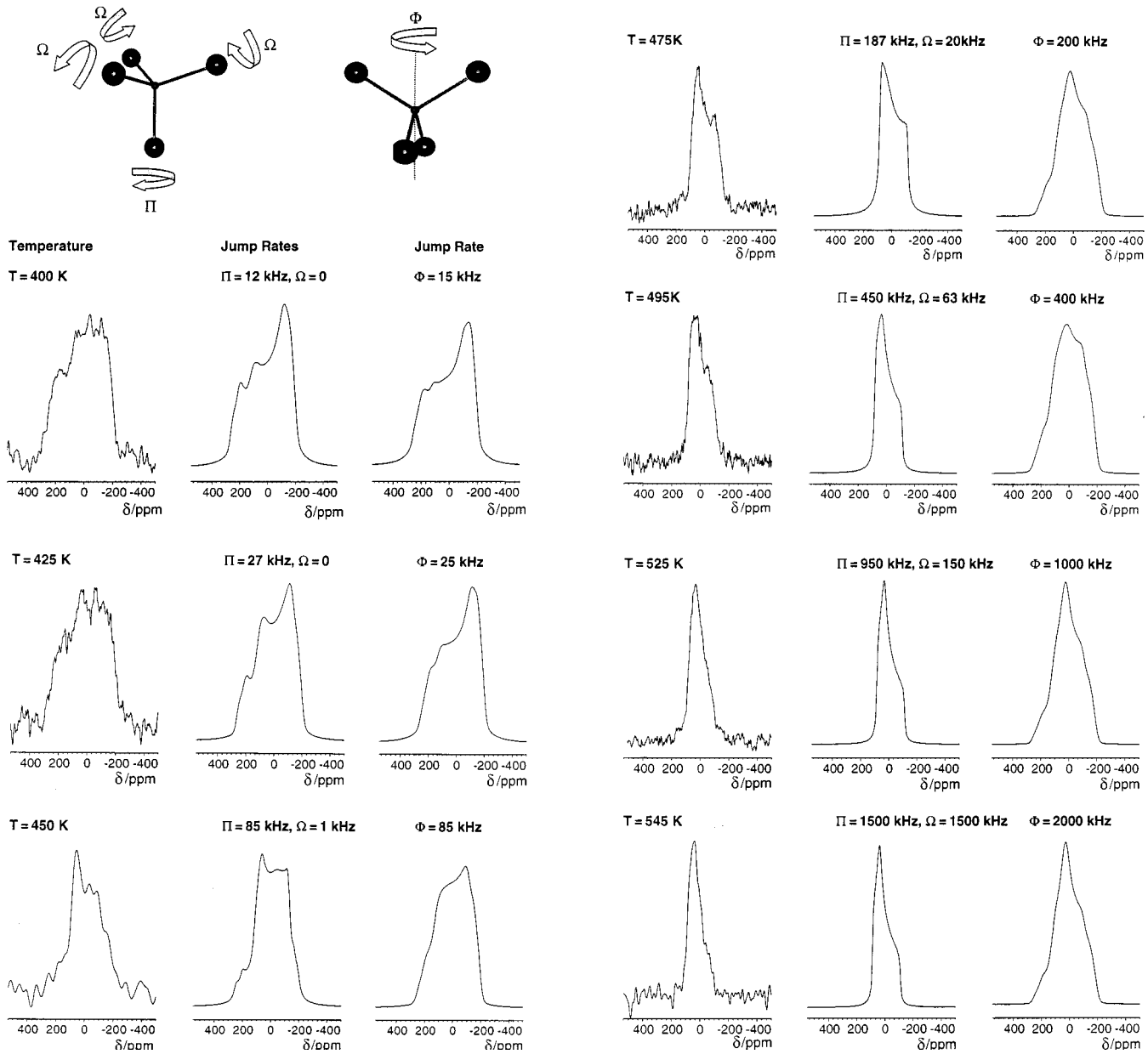

Figure 12. Comparison of the experimental ^{17}O NMR line shapes (left panel in each set of three) with simulations for two reorientational models shown: 3-fold reorientation with two distinct rates Π and Ω (middle panel in each set of three) and 2-fold reorientation with rate Φ (right panel in each set of three).

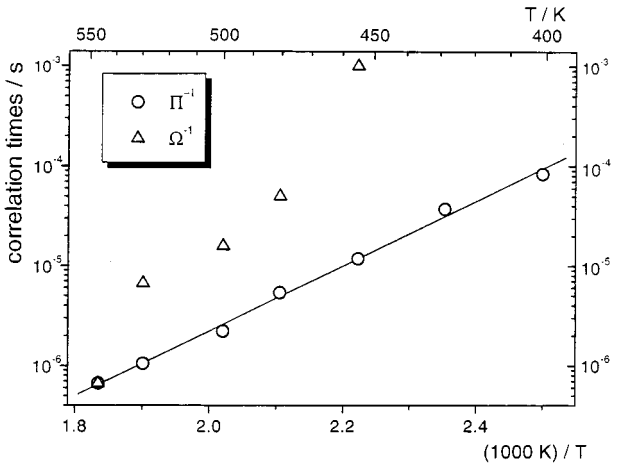

Figure 13. Arrhenius plot of the reorientation rates Π and Ω.

residual anisotropy would be retained in the ^{17}O spectra, even in the fast limit. The appearance of the isotropic line shape component shows that some PO_4^{3-} tetrahedra are in a state of rapid reorientation of the rotational axis, hence indicating anionic dynamics not unlike the situation in the high-temperature phase. The analogous situation is seen in the ^{23}Na NMR spectra above 525 K. The strong correlation observed here for both anions and cations lends further support to the idea of a dynamic coupling between anion and cation motion in the low-temperature phase: specifically, it suggests that above 525 K, the crystal structure is forming domains in which the orientational ordering of the phosphate ions has broken down completely and where the local cation and anion mobility is comparable to that observed in the high-temperature phase. As the temperature is raised further, Figures 5 and 8 illustrate that the number of such domains and/or their size begins to grow continuously. This domain model is nicely consistent with the abrupt change in the volume expansion coefficient, which begins at 525 K (see Figure 9); furthermore, the appearance of excess specific heat becomes clearly noticeable at these temperatures. This behavior is similar to that observed in $LiNaSO_4$, in which

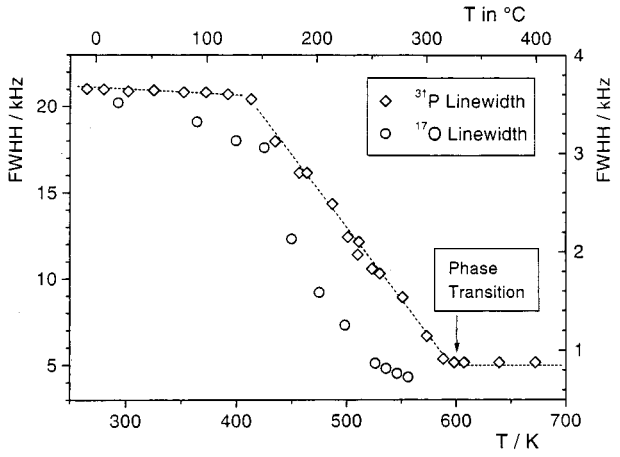

Figure 14. Temperature dependence of the ^{17}O and ^{31}P NMR line widths (full width at half-maximum) in LT-Na_3PO_4.

premonitory effects indicate the approach of the phase transition to the plastic crystalline form.[25] In this case the anomalous volume increase in the low-temperature phase correlates with pronounced nonlinear behavior of the atomic displacement parameters due to strong anharmonic thermal vibration of the atoms such as anion rotation.[26] Since the thermal expansion in ionic salts is mainly determined by the anharmonicity of the cation−anion interactions, the observed reorientational motion of the phosphate anions and their coupling with sodium motion strongly suggest a correlation between the structural and dynamic changes in the course of the phase transition.

In addition, the diffuse intensities in LT-Na_3PO_4 diffraction patterns at the position of the strongest cubic Bragg reflection also reveal residual local cubic clusters of sufficient coherence length to produce distinct diffraction peaks down to room temperature. From structural and thermodynamical considerations the obstruction of lattice relaxation may result from very small amounts of impurities, which apply strain to their local surrounding and hence conserve the local cubic symmetry. Such local disordered cubic clusters, which become potential embryos of the cubic high-temperature phase with increasing temperature, would give a proper explanation for the classical first-order character of the phase transition in terms of nucleation theory. According to this a sufficient amount of thermal energy is required to overcome the activation energy barrier and achieve the critical domain size for the formation of the high-temperature phase. This is highlighted by the fact that the phase transition shows typical hysteresis effects up to 20 K superheating.

Conclusions

In summary, the details of both anion and cation motion in LT-Na_3PO_4 have been characterized by temperature-dependent ^{17}O, ^{23}Na, and ^{31}P line shape and nutation NMR studies. The results suggest strong dynamic coupling between the reorientation of the PO_4^{3-} ions about their 3-fold axes and the translational diffusion of the Na^+ ions. The combined NMR, DSC, and XRD results also give interesting insights into the nature of the phase transition to the cubic high-temperature phase at 600 K. About 75 K below the phase transition temperature, locally cubic domains appear in the structure, in which the atomic and molecular dynamics of anions and cations are similar to those in the high-temperature phase. The NMR data indicate that the volume fraction of these domains increases with increasing temperature, thereby explaining the anomalously large volume expansion coefficient observed within this temperature range.

Acknowledgment. This work was partially supported by the Deutsche Forschungsgemeinschaft under the Sonderforschungsbereichs Program SFB458. Additional financial help from the Wissenschaftsministerium Nordrhein-Westfalen and from the Fonds der Chemischen Industrie is gratefully acknowledged.We thank Professor Klaus Funke for helpful discussions.

References and Notes

(1) Kvist, A.; Bengtzelius In *Fast Ion Transport in Solids*; van Gool, W., Ed.; North-Holland: Amsterdam, 1973; p 193.
(2) Lundén, A. *Solid State Ionics* **1988**, *28−30*, 163.
(3) Lundén, A. *Solid State Commun.* **1988**, *65*, 1237.
(4) Lundén, A.; Dissanayake, J. *Solid State Chem.* **1991**, *90*, 179.
(5) Lundén, A. *Solid State Chem.* **1993**, *107*, 296.
(6) Lundén, A. *Solid State Ionics* **1994**, *68*, 77.
(7) Secco, E. *Solid State Ionics* **1988**, *28−30*, 168.
(8) Secco, E. *Solid State Ionics* **1991**, *45*, 335.
(9) Secco, E. *J. Solid State Chem.* **1992**, *96*, 366.
(10) Secco, E. *Solid State Ionics* **1993**, *60*, 233.
(11) Jansen, M. *Angew. Chem.* **1991**, *103*, 1574.
(12) Funke, K.; Wilmer, D.; Witschas, M.; Banhatti, R.; Lechner, R. E.; Fitter, J.; Korus, G.; Jansen, M. *Mater. Res. Soc. Symp. Proc.* **1998**, *527*, 469.
(13) Witschas, M.; Eckert, H.; Wilmer, D.; Banhatti, R. D.; Funke, K.; Fitter, J.; Lechner, R. E. *Z. Phys. Chem.* **2000**, *214*, 643.
(14) Lissel, E.; Jansen, M.; Jansen, E.; Will, G. *Z. Kristallogr.* **1990**, *192*, 233.
(15) M. Witschas, U. Pingel, and H. Eckert, manuscript in preparation.
(16) Van Vleck, J. H. *Phys. Rev.* **1948**, *74*, 1168.
(17) Freude, D.; Haase, J. *NMR: Basic Princ. Prog.* **1993**, *29*, 1.
(18) Masuda, Y.; Sano, M.; Yamatera, H. *J. Chem. Soc., Faraday Trans. 1* **1985**, *81*, 127.
(19) Abragam, A. *Principles of Nuclear Magnetism*; Clarendon Press: Oxford, U.K., 1961.
(20) Spiess, H. W.; Sillescu, H. *J. Magn. Reson.* **1981**, *42*, 381.
(21) Spiess, H. W. *Chem. Phys.* **1974**, *6*, 217.
(22) Greenfield, M. S.; Ronemus, A. D.; Vold, R. L.; Vold, R. R. *J. Magn. Reson.* **1987**, *72*, 89.
(23) Kentgens, A. P. M.; Lemmens, J. M. M.; Geurts, F. M. M.; Veeman, W. S. *J. Magn. Reson.* **1987**, *71*, 62.
(24) Wiench, D. M.; Jansen, M. Z. *Anorg. Allg. Chem.* **1980**, *461*, 101.
(25) Freiheit, H.-C.; Putnis, A.; Kroll, H. *Z. Kristallogr.* **1998**, *213*, 575.
(26) Freiheit, H.-C.; Kroll, H.; Krane, H.-G.; Kirfel, A. HASYLAB Annual Report 1999.